7-25-2008

An Interactive Bayesian Geostatistical Inverse Protocol for Hydraulic Tomography

Michael N. Fienen
Wisconsin Water Science Center, U.S. Geological Survey

Tom Clemo
Boise State University

Peter K. Kitanidis
Stanford University

 DOI: 10.1029/2007WR006730

An interactive Bayesian geostatistical inverse protocol for hydraulic tomography

Michael N. Fienen,[1] Tom Clemo,[2] and Peter K. Kitanidis[3]

Received 3 December 2007; revised 5 March 2008; accepted 14 April 2008; published 25 July 2008.

[1] Hydraulic tomography is a powerful technique for characterizing heterogeneous hydrogeologic parameters. An explicit trade-off between characterization based on measurement misfit and subjective characterization using prior information is presented. We apply a Bayesian geostatistical inverse approach that is well suited to accommodate a flexible model with the level of complexity driven by the data and explicitly considering uncertainty. Prior information is incorporated through the selection of a parameter covariance model characterizing continuity and providing stability. Often, discontinuities in the parameter field, typically caused by geologic contacts between contrasting lithologic units, necessitate subdivision into zones across which there is no correlation among hydraulic parameters. We propose an interactive protocol in which zonation candidates are implied from the data and are evaluated using cross validation and expert knowledge. Uncertainty introduced by limited knowledge of dynamic regional conditions is mitigated by using drawdown rather than native head values. An adjoint state formulation of MODFLOW-2000 is used to calculate sensitivities which are used both for the solution to the inverse problem and to guide protocol decisions. The protocol is tested using synthetic two-dimensional steady state examples in which the wells are located at the edge of the region of interest.

Citation: Fienen, M. N., T. Clemo, and P. K. Kitanidis (2008), An interactive Bayesian geostatistical inverse protocol for hydraulic tomography, *Water Resour. Res.*, *44*, W00B01, doi:10.1029/2007WR006730.

1. Introduction and Background

[2] A principal challenge in hydrogeology is the need to obtain details on characteristics and properties of an aquifer over potentially large areas. The installation of wells is expensive and often constrained by surface construction, property access considerations, and a host of other issues. Best approaches are those that make the most of the data available within the context of errors. Early aquifer characterization was based on pumping tests performed in a single well (converging radial flow), assuming a homogeneous aquifer, and with various other assumptions, fitting an analytical solution to the drawdown curve. This work began with *Slichter* [1899] and *Thiem* [1906] for steady state and *Theis* [1935] extended it to transient conditions. Compendia of special cases under various conditions are presented in textbooks [e.g., *Batu*, 1998; *Kruseman and De Ridder*, 1990]. These solutions provide a homogeneous bulk average of the target hydraulic parameter. However, no medium is truly homogeneous and even subtle heterogeneity can play an important role in interpreting flow, and especially transport behavior [see, e.g., *Mackay et al.*, 1986; *Freyberg*, 1986]. *Liu et al.* [2007] also showed that even correct mean hydraulic parameters cannot correctly predict drawdown based on pumping tests at different locations in the domain. To better simulate the system of interest, models have grown in complexity with increasing numbers of nodes at a pace constrained mostly by advances in computational power. Often the number of nodes in a model greatly exceeds the available number of measurements resulting in an underdetermined problem. Methods that incorporate prior information or enforce a structure on the parameters result in an even-determined problem and the Bayesian geostatistical approach adopted in this work is such a method.

[3] In this work, we illustrate the value of a flexible approach to the inverse problem. Specifically, zonal boundaries are inferred from observations assisted by a small but important amount of prior information. In the examples we evaluate, perfect correspondence between model predictions and observations can be obtained if the boundaries of homogeneous zones are known in advance, but the real power of the method employed herein is in both determining where zonal boundaries are located, and the level of complexity that should be present within each zone. We also contend that, rather than being a black box, inverse modeling is an interactive process requiring judgment from the practitioner at several steps.

[4] *Yeh and Lee* [2007] recently argued that a paradigm shift in aquifer characterization, using methods that allow for more detailed parameterization, is essential and imminent. We agree and contend that for many studies the information available from wells is underutilized when used only to estimate hydraulic parameters for one or very few

[1]Wisconsin Water Science Center, U.S. Geological Survey, Middleton, Wisconsin, USA.
[2]Center for Geophysical Investigation of the Shallow Subsurface, Boise State University, Boise, Idaho, USA.
[3]Civil and Environmental Engineering, Stanford University, Stanford, California, USA.

0043-1397/08/2007WR006730$09.00

homogeneous zones. *Li et al.* [2007] showed that hydraulic parameter values obtained from fitting *Theis* [1935] curves to data from individual pumping tests at multiple locations and interpolating results does not correctly characterize the heterogeneous distribution although the mean parameter values are calculated correctly. Similarly, *Straface et al.* [2007] illustrated that sequential testing with a distributed groundwater inverse model often yields a more geologically realistic characterization. Inverse modeling allows multiple measurements of drawdown or head change to guide the estimation of hydraulic parameters. The inverse problem, however, is typically underdetermined with many more unknown parameters (i.e., hydraulic conductivity values in grid cells for the model) than measurements (drawdown values at a limited number of wells, for a limited number of pumping tests). Underdetermined problems do not have a unique solution. This shortcoming can be overcome either by collecting more measurements until they equal or exceed the number of parameters to estimate, by effectively decreasing the number of parameters through lumping, or by constraining the solution using Bayes' theorem and the inclusion of prior information.

[5] As *Yeh and Lee* [2007] suggest, rather than installing more wells to reduce the ratio of parameters to observations, multiple pumping tests or "stimulation events" can be performed using various configurations of existing wells. The pumping/drawdown response from the series of tests can form a single inverse problem that can be solved to find the set of hydraulic parameters that best represents the observations from all the tests simultaneously. This technique has been called hydropulse tomography [*Tosaka et al.*, 1993], a sequential aquifer test [e.g., *Liu et al.*, 2002], or more commonly hydraulic tomography [*Bohling*, 1993; *Gottlieb and Dietrich*, 1995]. Hydraulic tomography developed at the confluence of techniques in several fields. Tomographic methods have a long history in geophysics [*Sharma*, 1997] using seismic, electric current, or radar wave propagation through an aquifer to constrain inversion of petrophysical properties. By analogy, the propagation of water pressure waves can be used to recover hydraulic properties [*Tosaka et al.*, 1993; *Vasco et al.*, 2000; *Brauchler*, 2005]. Several methods of incorporating this information into the groundwater inverse problem have been proposed, including direct inversion of head data [*Tosaka et al.*, 1993; *Gottlieb and Dietrich*, 1995; *Butler et al.*, 1999; *Yeh and Liu*, 2000], steady shape analysis [*Bohling et al.*, 2002], asymptotic streamline inversion [*Vasco and Datta-Gupta*, 1999], and matching temporal moments of drawdown [*Li et al.*, 2005; *Zhu and Yeh*, 2006]. Recent work on both sandbox models [*Illman et al.*, 2007; *Liu et al.*, 2007] and a field application [*Li et al.*, 2007] highlight the power of hydraulic tomography in general, and a Bayesian-based parameter estimation approach specifically. The main contribution of the present work is in illustrating the importance that discontinuities in hydraulic conductivity, even of only a single order of magnitude, can impart on the solution of a hydraulic tomography inverse problem. In the following sections, we discuss methods to determine and evaluate zonation candidates to obtain the best parameter estimation given the available data.

[6] Another motivation for hydraulic tomography is the notion that each pumping test location in an aquifer focuses interrogation on a different part of the aquifer. *Giudici et al.* [1995] examined the value of combining multiple stimulations of an aquifer to refine distributed transmissivity estimates. Multiple pumping tests with a small network of wells can be much more informative than a single pumping test with a much larger network of observation wells [*Snodgrass and Kitanidis*, 1998]. Even with only two wells, *Kunstmann et al.* [1997] showed improved characterization when performing unequal strength dipole pumping tests using one well as a source and the other as a sink, and then reversing the configuration. The specific configuration of injection, extraction, and monitoring wells in the field impacts the informative coverage. In the context of dispersivity evaluation, *Tiedeman and Hsieh* [2004] explored the differences among single-well converging radial pumping tests and equal and unequal strength dipole tests. Although their focus was on the characterization of dispersivity under different flow conditions, they also highlighted the different areas of an aquifer interrogated under the various flow conditions.

[7] In this work, we present a protocol for implementing hydraulic tomography, and propose an interactive inversion scheme using Bayesian geostatistical inverse theory as the kernel. Prior information about aquifer parameter characteristics enforces a level of smoothness or continuity in the parameter field. By "interactive" we mean that aquifer structure, rather than being fixed a priori, is identified through the inversion process and is evaluated by the modeler multiple times both through the inclusion of prior information and the selection of zones. This interactive aspect is motivated by recognition that inverse methods should not be applied as a black box but rather that modelers must be involved and make decisions impacting the results throughout the process. Intermediate results are examined to explore the impact various selections of both structural parameters (the variogram parameters characterizing the nature of prior information) and zonation candidates have on the solution. This probabilistic approach imposes minimal prior assumptions on the parameters, allowing pertinent information contained within the data to drive the solution and explicitly accounting for uncertainty.

[8] Uncertainty is introduced both through epistemic uncertainty and our inability to fully characterize inherent variability of the media we model. Epistemic uncertainty, which is the error introduced by imperfect and sparse measurements, roundoff error, approximations of models, and conceptual model errors, can be reduced but never fully removed by improving models and collecting more and better data. An epistemic error term accounts for the presence of epistemic uncertainty in the inversion. Inherent variability, or the heterogeneity of parameters in the aquifer, cannot be reduced but is accounted for through prior covariance.

[9] The Bayesian geostatistical inverse approach to hydraulic conductivity identification is usually performed assuming a constant but unknown mean about which the best estimate varies [e.g., *Hoeksema and Kitanidis*, 1984; *Snodgrass and Kitanidis*, 1998]. In some applications, however, it may be more appropriate to use a variable mean if a prior trend is justified [*Kitanidis*, 1997], or to include diffuse information about the mean [*Nowak and Cirpka*, 2004]. Taking this concept further, the known hydrogeology of the

site may indicate segregation into zones with independent means that may improve the solution. For example, in the inversion of electromagnetic borehole flowmeter data, significant improvement was obtained by assigning zonal boundaries on the basis of a sharp contact between highly contrasting hydraulic conductivity zones [*Fienen et al.*, 2004]. In some cases, prior knowledge such as discrete layering [*Bohling et al.*, 2007], geophysical results [*Hyndman et al.*, 2000], or other information may guide the selection of zone boundaries.

[10] It is critical to acknowledge that once such boundaries are defined, they act as strong constraints on the solution, so care must be taken to justify the placement of zones. Ideally, the data that directly constrain the inversion can also provide enough information to indicate an appropriate zonation scheme. Exploiting such information empowers the data to drive the inversion. In this work, we assume only that a practitioner suspects the presence of sharp contacts, and some expert knowledge is employed to select zones on the basis of interrogation of the best estimate first obtained assuming a constant mean. Practitioners then select among several candidates for appropriate zonations and are guided toward final selection of a best candidate using metrics based on examination of orthonormal residuals as proposed by *Kitanidis* [1991, 1997].

[11] Given N distinct screened intervals that can be used either for pumping or observation, there are two main strategies for performing the pumping tests and obtaining the observations to be used for hydraulic tomography. The first strategy is to pump each well in turn while monitoring all the other wells. The second strategy is to perform a sequence of dipole tests in which water is injected into one well and extracted out of another at the same rate. Again, the pressure is observed in every well not being pumped. The former is referred to as "single well hydraulic tomography" (SHT) and the latter as "dipole hydraulic tomography" (DHT). The number of possible stimulation events in the field for SHT is N resulting in N $(N - 1)$ head observations. For DHT, there are $\frac{N(N-1)}{2}$ combinations of dipoles resulting in $\frac{N(N-1)(N-2)}{2}$ head observations.

[12] The number of stimulation events translates directly into the number of forward model runs. Thus, for a given number of wells, much more data may be obtained using DHT. The cost of installing wells is greater than the cost of performing pumping tests, so performing as many tests as practical with a given well field should lead to the best characterization possible. For a given level of epistemic uncertainty attributed to each measurement, the greater number of data obtained with dipoles rather than single well tests can average out measurement errors thus reducing uncertainty. Furthermore, dipoles are expected to reach steady state faster than single well tests, so we explore DHT in the synthetic examples of this work.

[13] The progression from a set of field observations to a best estimate of the hydraulic conductivity field is guided by a combination of sensitivity analysis of observations to parameters, the degree of prior information weighting, and the selection of zones. The interpretation of the solution to the geostatistical inverse problem as a mapping of observations into parameter space through the use of stochastic "splines" was discussed by *Kitanidis* [1998] and further explored in the context of multiple pumping tests by *Snodgrass and Kitanidis* [1998]. For a large number of wells, it may be infeasible to perform all possible configurations of pumping tests to fully realize the potential benefit of employing the DHT protocol. Sensitivity matrices, discussed in section 6, may identify redundant information resulting from some of the dipoles, or one may simply select a subset of all dipole configurations to use. Three synthetic examples are included: a stationary heterogeneous field and two fields of homogeneous hydraulic conductivity that contain inclusions. The stationary heterogeneous field serves as a demonstration model under ideal conditions while the contrast in the inclusion cases push the constant mean assumption to its limit and illustrates the value of using zonation to provide for different mean values in distinct zones.

2. Statement of the Problem

[14] The goal of this work is to perform hydraulic tomography using several pumping and observation wells to obtain a probabilistic estimate for a hydraulic conductivity field. Because the probabilistic estimate is formulated to consider inherent variability and epistemic uncertainty, it provides a direct measure of uncertainty about the most probable estimate. Using steady state tests, a Bayesian geostatistical inverse approach is applied to the problem. Prior information is limited to the location of well screens available for pumping and drawdown observations, selection of an appropriate generalized covariance function used in the prior covariance for the inversion, and a zonation assumption. Selection of the generalized covariance function model is based on the general presumed characteristics (e.g., smoothness or continuity) of the parameter field. The data dictate selection of the parameters for the covariance model which determines the degree to which this characteristic is enforced. The initial zonation assumption is a single unknown mean (i.e., a single zone). The role of the prior covariance and the estimation of its structural parameters are discussed below. For this work, an exponential generalized covariance function is used with a large integral scale to allow the function to mimic a linear covariance function while behaving as an appropriate stationary covariance.

[15] The stimulation events are performed at steady state in two dimensions. The forward model used to generate synthetic observations and to solve the inverse problem is MODFLOW-2000 (MODFLOW) [*Harbaugh et al.*, 2000]. An adjoint state version of MODFLOW is applied to calculate sensitivity matrices [*Clemo*, 2007].

[16] In steady state inversion, the aquifer must recover from each stimulation event to ensure that the observations from one test are not impacted by conditions still changing from the previous test. Over the course of a field experiment it may be difficult to isolate an aquifer from all impacts of regional conditions such as distant pumping activity, evapotranspiration, or recharge. Assuming that regional conditions are steady state over the long term can introduce significant uncertainty and error in the estimation of parameters. Therefore we formulate the governing equations more generally to mitigate changing system state. If regional conditions change at a timescale slower than an individual stimulation, but faster than the duration of an entire hydraulic tomography experiment, this uncertainty can be

reduced by working with drawdown rather than head values. By controlling the conditions under which data are collected the data value is increased and uncertainty is reduced.

[17] Consider the governing equation of groundwater flow for a steady state isotropic condition [*Fetter*, 1994]

$$\nabla \cdot (K(\mathbf{x})\nabla\phi_0) = -R(\mathbf{x}) \tag{1}$$

$$\text{with } \phi_0 = \phi_b \text{ on the boundary } \Gamma \tag{2}$$

where $K(\mathbf{x})$ is hydraulic conductivity, $\mathbf{x}$ is a position vector, ϕ_0 and ϕ_b are hydraulic head and $R(\mathbf{x})$ is the preexistent recharge. All these variables are spatially variable.

[18] Next, the system is stimulated through pumping in wells or any other stimulation, expressed as a function of space on the right hand side:

$$\nabla \cdot (K\nabla\phi_1) = f(\mathbf{x}) - R(\mathbf{x}) \tag{3}$$

$$\text{with } \phi_1 = \phi_b \text{ on the boundary } \Gamma \tag{4}$$

where $f(\mathbf{x})$ is a spatial function including all stimuli, and $R(\mathbf{x})$ remains as the preexistent recharge.

[19] If we are interested in the quantity $\phi_D \triangleq (\phi_1 - \phi_0)$ then, by superposition, we can subtract the previous two equations

$$\nabla \cdot (K\,\nabla(\phi_D)) = f(\mathbf{x}) - R(\mathbf{x}) - (-R(\mathbf{x})) = f(\mathbf{x}) \tag{5}$$

$$\text{with } \phi_D = 0 \text{ on the boundary } \Gamma \tag{6}$$

[20] In this way, provided that ϕ_b and $R(\mathbf{x})$ are constant over the timescale of $f(\mathbf{x})$, we are left with a problem that is independent of boundary conditions including uncontrolled recharge and regional flow. Rather than measuring and simulating head relative to a constant datum, the head measured in each well at the start of each stimulation event serves as the datum for that event. For the observation data, we then use drawdown (head difference) rather than head. This is consistent with equations (5) and (6). Previous hydraulic tomography applications have used drawdown rather than raw head data [see e.g., *Li and Cirpka*, 2006], although they were motivated by the need for integratable data to calculate moments for transient data and do not discuss the impact of regional conditions. Steady shape conditions described by *Bohling et al.* [2002] provide another useful alternative intermediate between transient and steady state conditions.

[21] To implement the steady state method outlined above, changes in regional conditions must occur on a timescale slower than the individual pumping stimulation event. The regional conditions may be different for each stimulation, but over the course of an individual stimulation, they should be effectively constant. Dipoles may reach steady state conditions more rapidly.

3. Bayesian Geostatistical Inversion: The Quasi-linear Approach

[22] The inverse method used in this work is the Bayesian geostatistical inverse method [e.g., *Hoeksema and Kitanidis*, 1984; *Kitanidis*, 1995]. A summary of the derivation follows.

3.1. Bayes' Theorem

[23] This method is rooted in Bayes' theorem, which states

$$p(\mathbf{s}|\mathbf{y}) \propto L(\mathbf{y}|\mathbf{s})\, p(\mathbf{s}) \tag{7}$$

where $p(\mathbf{s}|\mathbf{y})$ is the posterior probability density function (pdf) of the unknown parameters ($\mathbf{s}$), $L(\mathbf{y}|\mathbf{s})$ is the conditional pdf of the observations ($\mathbf{y}$) given the parameters, referred to as the likelihood function, and $p(\mathbf{s})$ is the prior pdf. We assume these pdfs to be multi-Gaussian although this assumption can be relaxed using more computationally intensive Markov chain Monte Carlo methods [e.g., *Michalak and Kitanidis*, 2003; *Fienen et al.*, 2006]. The prior pdf contains limited assumptions about the structure of the parameter field prior to the experiments being performed and measurements being made. The likelihood function provides the means to update this prior information with the results of experiments and/or measurements, yielding the posterior pdf. The posterior pdf provides the best estimate and an estimate of uncertainty in the parameters conditional upon both the prior information and the experiments or data analysis.

[24] Using a probabilistic approach acknowledges the nonuniqueness of the parameter estimation problem and incorporates uncertainty from multiple sources into the process expressed in the posterior pdf. It is also possible to estimate posterior uncertainty of the estimated parameters, although these results are not presented in this work. *Kitanidis* [1995] describes the calculation of posterior covariance necessary to quantify posterior uncertainty.

3.1.1. Prior Probability Density Function

[25] The prior pdf of $\mathbf{s}$ ($p(\mathbf{s})$ in equation (7)) can be characterized through its mean and covariance. We model $\mathbf{s}$ as a random process with mean

$$E[\mathbf{s}] = \mathbf{X}\beta \tag{8}$$

where $E[\cdot]$ indicates expected value, β is a vector of unknown drift parameters ($p \times 1$) and $\mathbf{X}$ is an ($m \times p$) matrix of base functions. The matrix $\mathbf{X}$ associates each of the m values of $\mathbf{s}$ with the appropriate element of β, and can express zonation or trend information known a priori about $\mathbf{s}$. For a problem with a single, constant mean, $\mathbf{X}$ is simply an ($m \times 1$) vector of ones. For a problem with multiple zones, each with a corresponding mean value β_j, $\mathbf{X}$ is an assignment matrix where X_{ij} is 1 if the parameter i is in the zone with the jth mean value β_j, and is zero otherwise.

[26] To enforce nonnegativity of $\mathbf{s}$ in unconstrained optimization it is advantageous to work with the logarithm of hydraulic conductivity

$$\mathbf{s} = \ln \mathbf{k} \tag{9}$$

where $\mathbf{k}$ is the hydraulic conductivity vector.

[27] The prior covariance ($\mathbf{Q}$) of $\mathbf{s}$ is

$$\mathbf{Q}(\theta) = E\left[(\mathbf{s} - \mathbf{X}\beta)(\mathbf{s} - \mathbf{X}\beta)^T\right] \tag{10}$$

This approach is an empirical Bayes technique, so a model of $\mathbf{Q}(\theta)$ must be specified a priori (e.g., a variogram type),

but the parameters (e.g., the variogram parameters, θ) are estimated on the basis of the data. For the remainder of this section, $\mathbf{Q}(\theta)$ is assumed known, and the selection of the specific model for $\mathbf{Q}(\theta)$ and its parameters (θ) are discussed in the next section.

[28] Assuming a Gaussian distribution, the prior pdf is

$$p(\mathbf{s}) = \frac{1}{\sqrt{(2\pi)^m \det(\mathbf{Q})}} \exp\left[-\frac{1}{2}(\mathbf{s}-\mathbf{X}\beta)^T \mathbf{Q}^{-1}(\mathbf{s}-\mathbf{X}\beta)\right] \quad (11)$$

where det (·) is the matrix determinant.

3.1.2. Likelihood Function

[29] The likelihood function ($L(\mathbf{y}|\mathbf{s})$ in equation (7)) is a measure of misfit between predictions of the measurements made for a specific set of parameter values weighted by epistemic uncertainty. The measurement equation relates the observations to the unknown parameters

$$\mathbf{y} = \mathbf{h}(\mathbf{s}) + \mathbf{v} \quad (12)$$

where $\mathbf{y}$ is an ($n \times 1$) vector of observations (drawdown measurements), $\mathbf{s}$ is an ($m \times 1$) vector of unknown parameters (log hydraulic conductivity), $\mathbf{h}(\mathbf{s})$ is a function or model that calculates predictions corresponding to observation values as a function of $\mathbf{s}$, and $\mathbf{v}$ is an ($n \times 1$) vector of epistemic error terms, modeled as a random process with zero mean and covariance matrix $\mathbf{R}$. Epistemic uncertainty results from imperfect or sparse measurements and also an incomplete or inappropriate conceptual model. The epistemic error terms are assumed independent so $\mathbf{R}$ is calculated as

$$\mathbf{R} = \sigma_R^2 \mathbf{I} \quad (13)$$

where σ_R^2 is the epistemic uncertainty parameter and $\mathbf{I}$ is an $n \times n$ identity matrix. The model error contribution to epistemic uncertainty may, in reality, be systematic and correlated [*Gaganis and Smith*, 2001]. A significant source of model error is reduced when, as in this case, the scale of model nodes is smaller than the scale of heterogeneous variability in the parameters [*Gallagher and Doherty*, 2007]. Nonetheless, the decision to assume uncorrelated homoscedacticity in this work was made for practicality, and the matrix $\mathbf{R}$ can easily accommodate structure in the epistemic error covariance.

[30] The likelihood function is

$$L(\mathbf{y}|\mathbf{s}) = \frac{1}{\sqrt{(2\pi)^n \det(\mathbf{R})}} \exp\left[-\frac{1}{2}(\mathbf{y}-\mathbf{h}(\mathbf{s}))^T \mathbf{R}^{-1}(\mathbf{y}-\mathbf{h}(\mathbf{s}))\right] \quad (14)$$

3.1.3. Posterior Probability Density Function

[31] Applying Bayes' theorem, the posterior pdf is the product of equations (14) and (11). After some algebraic manipulation and removing constants, we can define an objective function that is equivalent to the negative logarithm of the posterior pdf

$$\mathcal{L} = (\mathbf{y}-\mathbf{h}(\mathbf{s}))^T \mathbf{R}^{-1}(\mathbf{y}-\mathbf{h}(\mathbf{s})) + \mathbf{s}^T \mathbf{G}\mathbf{s} \quad (15)$$

where

$$\mathbf{G} = \mathbf{Q}^{-1} - \mathbf{Q}^{-1}\mathbf{X}\left(\mathbf{X}^T\mathbf{Q}^{-1}\mathbf{X}\right)^{-1}\mathbf{X}^T\mathbf{Q}^{-1} \quad (16)$$

[32] A computationally efficient method to find the best estimate is through superposition of the calculated mean and fluctuations

$$\hat{\mathbf{s}} = \mathbf{X}\hat{\boldsymbol{\beta}} + \mathbf{Q}\mathbf{H}^T\xi \quad (17)$$

where $\mathbf{H}$ is the sensitivity matrix. The vector of weights (ξ), and the vector of mean values $\left(\hat{\boldsymbol{\beta}}\right)$ are found through the cokriging equations

$$\begin{bmatrix} \boldsymbol{\Sigma} & \mathbf{HX} \\ (\mathbf{HX})^{\mathbf{T}} & \mathbf{0} \end{bmatrix} \begin{bmatrix} \xi \\ \hat{\boldsymbol{\beta}} \end{bmatrix} = \begin{bmatrix} \mathbf{y} \\ \mathbf{0} \end{bmatrix} \quad (18)$$

where $\boldsymbol{\Sigma} = \mathbf{HQH}^T + \mathbf{R}$, and $\mathbf{H} = \frac{\partial h(\mathbf{s})_i}{\partial s_j}$ is found using adjoint state calculations.

[33] Estimating hydraulic conductivity from observations of head, $\mathbf{h}(\mathbf{s})$ is nonlinear so we expand the solution about a current best estimate $\tilde{\mathbf{s}}$. Following the quasi-linear approach of *Kitanidis* [1995]

$$\mathbf{h}(\mathbf{s}) \approx \mathbf{h}(\tilde{\mathbf{s}}) + \tilde{\mathbf{H}}(\mathbf{s}-\tilde{\mathbf{s}}) + HOT \quad (19)$$

where *HOT* are higher-order terms that are disregarded and $\tilde{\mathbf{H}}$, as a function of $\tilde{\mathbf{s}}$ must be recalculated at each linearization step.

[34] Updating the cokriging equations (equation (18)),

$$\begin{bmatrix} \boldsymbol{\Sigma} & \tilde{\mathbf{H}}\mathbf{X} \\ (\tilde{\mathbf{H}}\mathbf{X})^{\mathbf{T}} & \mathbf{0} \end{bmatrix} \begin{bmatrix} \xi \\ \hat{\boldsymbol{\beta}} \end{bmatrix} = \begin{bmatrix} \mathbf{y} - \mathbf{h}(\tilde{\mathbf{s}}) + \tilde{\mathbf{H}}\tilde{\mathbf{s}} \\ \mathbf{0} \end{bmatrix} \quad (20)$$

[35] Each iteration of this algorithm results in a new estimate of $\hat{\mathbf{s}}$ using equation (17) with ξ and $\hat{\beta}$ calculated using equation (20) and an updated computation of $\tilde{\mathbf{H}}$ For the next iteration, we replace $\tilde{\mathbf{s}}$ with $\hat{\mathbf{s}}$, and find a new $\hat{\mathbf{s}}$. Convergence is declared once $\|\mathcal{L}(\hat{\mathbf{s}}) - \mathcal{L}(\tilde{\mathbf{s}})\|_2$ or $\|\hat{\mathbf{s}} - \tilde{\mathbf{s}}\|_2$ decreases to a small tolerance, where $\|\cdot\|_2$ indicates an L-2 norm.

[36] In underdetermined inverse problems, such as this one, adjoint state calculations dramatically increase the efficiency of calculating the sensitivity matrix $\mathbf{H}$ which is calculated multiple times throughout the inversion process. Derivations of the adjoint state equations are given by *Sykes et al.* [1985] and *Sun* [1994]. Recall that n indicates the number of observations and m indicates the number of parameters. The end result is a formulation that calculates $\mathbf{H}$ using $n+1$ model runs rather than the $m+1$ or $2m+1$ runs required by the sensitivity equation or traditional perturbation sensitivities. The sensitivity matrix is calculated in physical space $\left(H_{ij} = \frac{\partial h_i}{\partial k_j}\right)$ but when we perform the forward calculation, we must convert to estimation space $\left(H_{ij} = \frac{\partial h_i}{\partial s_j}\right)$ in which the parameters are log transformed. This is accomplished using the chain rule

$$H_{i,j} = \frac{\partial h_i}{\partial k_j}\frac{\partial k_j}{\partial s_j} = \frac{\partial h_i}{\partial k_j}\frac{\partial \exp(s_j)}{\partial s_j} = \frac{\partial h_i}{\partial k_j}\exp(s_j) \quad (21)$$

[37] The adjoint state calculations are implemented in a modified version of MODFLOW. *Clemo* [2007] provides the derivation of the equations and implementation details used for adjoint state in MODFLOW. The savings in computational effort are greater than tenfold using the adjoint state method instead of finite differences in the synthetic cases described below. Most of the savings comes from the fact that m = 324 while n = 60, but additional overhead savings are achieved by performing the adjoint calculations in a single call to the program. In many applications, m is even greater than n and the advantage to using adjoint state is more significant.

3.2. Prior Covariance

[38] The prior covariance in geostatistical inversion is expressed through either a variogram covariance model or a generalized covariance function. In many random fields, this covariance model is adequate to handle the variability of the field, allowing for clusters of similar values rising above or dipping below the mean in a continuously varying field. Alternatively, sharp discontinuities may indicate zones of different mean values which are difficult to model with a single covariance and mean zone assumption. In the following subsections we first discuss the general covariance models to be used regardless of zonation followed by a discussion of incorporation of zones.

3.2.1. Prior Covariance Without Zones

[39] In this work, we adopt the exponential covariance model from which the linear covariance model can be approximated as a limiting case

$$R(h) = \sigma^2 \exp\left(-\frac{h}{\ell}\right) \tag{22}$$

where σ^2 is the variance, h is the separation distance (in absolute value) between nodes, and ℓ is the integral scale. A large integral scale suggests large pockets of similar parameter values, whereas a small integral scale indicates variability at a small scale allowing for a much rougher solution.

[40] The covariance model can be converted to a variogram

$$\gamma(h) = R(0) - R(h) = \sigma^2\left(1 - \exp\left(-\frac{h}{\ell}\right)\right) \tag{23}$$

[41] The generalized covariance function (GCF), $\kappa(h)$, is calculated as

$$\kappa(h) = -\gamma(h) + C \tag{24}$$

where C is an arbitrary constant. We may assume ℓ is large relative to h. In this case, variability takes place over the range of multiple nodes. At the limit as $\ell \to \infty$, $\exp\left(-\frac{h}{\ell}\right) \to 1 - \frac{h}{\ell}$. Substituting into equation (22)

$$R(h) = \sigma^2\left(1 - \frac{h}{\ell}\right) = \sigma^2 - \frac{\sigma^2}{\ell}h = \theta\ell - \theta h \tag{25}$$

where $\theta = \frac{\sigma^2}{\ell}$. Using this model, since $\ell > \max(h)$, the values will all be positive and the covariance matrix will be positive semidefinite and hence an authorized covariance. The corresponding variogram is the linear

$$\gamma(h) = R(0) - R(h) = \theta\ell - 0 - \theta\ell + \theta h = \theta h \tag{26}$$

[42] By assuming ℓ is constant and sufficiently large (we use 10 $\times$ max (h)), we can use equation (22) with the substitution of $\sigma^2 = \theta\ell$ as the prior covariance model

$$R(h) = \theta\ell \exp\left(-\frac{h}{\ell}\right) \tag{27}$$

[43] This model has the dual advantages of having a single parameter to estimate (θ, since ℓ is fixed as large) and it is a valid covariance. This allows us to set lack of correlation to zero.

[44] Adopting this GCF, $\mathbf{Q}$ in the prior pdf ($p(\mathbf{s})$) is

$$\mathbf{Q}(\theta) = \theta\ell \exp\left(-\frac{h}{\ell}\right) \tag{28}$$

3.2.2. Prior Covariance With Zones

[45] Splitting a domain into discrete zones is appropriate when the mean values of various subdomains are significantly different. Using the exponential generalized covariance function (GCF) with a large integral scale, sharp contrasts in conductivity are incompatible with the smoothly varying structure described by the prior covariance. However, sharp contrasts are common in hydrogeologic sedimentary environments in the form of geologic contacts, particularly at unconformities and paleostream channel boundaries. As a result, it is often beneficial to segregate the field into zones, each with its own mean and uncorrelated from each other. Determining the location of zones is difficult without a priori observations indicating where to draw the lines.

[46] The zones may be characterized by totally different covariance structures, or by a similar covariance structure with different mean values. Multiple θ parameters might also be necessary to characterize anisotropy in which correlation is described by direction-specific parameters. In both cases, restricted maximum likelihood or another alternative approach to finding θ must be implemented. In this work, we assume similar covariance structure in each zone but different means so a single parameter θ will apply to the same general covariance structure. The matrix $\mathbf{X}$ associates each zone with its appropriate element of $\hat{\beta}$ in equation (17). The $\mathbf{Q}$ matrix, calculated according to the specific GCF used, is censored such that for $Q_{ij} = 0$ when the ith and jth elements are in different zones and the zones are uncorrelated.

[47] In some cases, compelling information regarding zones is available in the form of boring logs, outcrop observations, or other data. Where such data are present, they should certainly be used to delineate zones and reliance on the inversion should be focused on estimating the parameters within the zones. Many approaches are available for incorporating outside information including multiple-

point geostatistics [*Caers and Zhang*, 2004; *Feyen and Caers*, 2006], indicator Kriging [*Journel*, 1983], or cluster analysis [*Tronicke et al.*, 2004; *Bohling et al.*, 2007]. Alternatively, there is often information in the data that can drive the selection of zones. For example, *Straface et al.* [2007] used inflections in observed drawdown curves, as suggested by *Oliver and Aramco* [1990] to indicate boundaries of different parameter zones. Minimum gradient support functionals can also be used in a penalization method to segregate a parameter field into zones. This approach is called ''image focusing'' in geophysics literature [*Portniaguine and Zhdanov*, 1999, 2002].

3.2.3. Thresholding to Select Zones

[48] A simplified version of image focusing is to examine thresholds within the best estimate of a nonzoned model. Our goal is to empower the data to drive the inversion, including the zonation. This approach allows us to start the inversion clear of preconceived notions of zonation candidates and use the observations to indicate appropriate zones. Zones are indicated by regions varying about different means. On a histogram, transitions between zones appear as gaps. The selection and definition of gaps is subject to expert interpretation, and several candidates are selected interactively. Metrics are derived below to guide final selection among these candidates. Therefore, a preliminary method to screen for zones is to divide a histogram of parameter values into a region above and a region below a threshold identified by a gap in the histogram. This is illustrated for a specific example in Figure 1a. This is an interactive, qualitative approach as several gaps may be present and expert knowledge is used to guide the number of zones and where to make cutoffs. For example, the very definition of a ''gap'' on the histogram is subject to interpretation. Furthermore, a practitioner may enforce more continuity or split zones by this method if soft information suggests such actions are appropriate. In this work, three candidates based on gap locations are made and the solutions are evaluated for each. The three candidate models were selected by a person unfamiliar with the project and instructed only to indicate three gaps in each histogram. The ultimate decision regarding which zonation candidate to adopt is based on cross validation results (section 4) and expert discretion.

[49] Figure 1a shows a candidate for zonation selected from the best estimate of a nonzoned solution using the method outlined above. $\mathbf{Q}_0$, the kernel of $\mathbf{Q}$, is independent of the structural parameter θ. For the linear generalized covariance function approximated by the exponential

$$\mathbf{Q}_0 = \ell \exp\left(-\frac{h}{\ell}\right) \tag{29}$$

[50] To enforce zonation, this kernel must be censored by setting all covariance matrix values in $\mathbf{Q}_0$ to zero if the two nodes are in different zones. Figure 2 shows two versions of the matrix $\mathbf{Q}_0$: the top without zonation, and the bottom split into three zones according to Figure 1a. $\mathbf{Q}$ is calculated as $\theta \times \mathbf{Q}_0$. Additionally, $\mathbf{X}$ must be created such that nodes are mapped to the appropriate means as discussed in section 3.1.1. For each zonation candidate, the geostatistical model will be different, and the structural parameters, θ, will need to be estimated uniquely.

4. Structural Parameters

[51] Two structural parameters must be estimated along with the values of hydraulic conductivity in the model nodes: the epistemic error parameter (σ_R^2 in equation (13)), and the prior covariance model parameter (θ in equation (28)). These two parameters are estimated through examination of orthonormal residuals [*Kitanidis*, 1991, 1997]. If the structural parameters are appropriate, the drawdown residuals should have zero mean and little spread about the mean. *Kitanidis* [1991] suggested two metrics to evaluate structural parameters using orthonormal residuals $\left(\frac{\delta_i^2}{\sigma_i^2}\right)$:

$$Q_2 = \frac{1}{n-p}\sum_{k=p+1}^{n}\frac{\delta_k^2}{\sigma_k^2} \tag{30}$$

and

$$cR = Q_2 \times \exp\left(\frac{1}{n-p}\sum_{i=p+1}^{n}\ln\left(\sigma_i^2\right)\right) \tag{31}$$

where n is the number of measurements, p is the number of hydraulic conductivity drift parameters, δ are the residuals (the actual errors between observations and predictions of drawdown), and σ are the estimation variances. We seek parameters that minimize cR with the constraint that $Q_2 = 1$. This is most easily accomplished by selecting a value for σ_R^2 and varying θ over several orders of magnitude. It is easier, a priori, to determine a reasonable value for σ_R^2 than for θ since epistemic errors are related to measurement errors for which there may be estimates. Otherwise, setting σ_R^2 to 10% of the mean drawdown value is a reasonable starting value.

[52] The ratio of $\frac{\theta}{\sigma_R^2}$ controls the trade-off between fitting the observations and enforcing prior information. Small values of $\frac{\theta}{\sigma_R^2}$ produce smoother parameter fields. The optimal ratio of $\frac{\theta}{\sigma_R^2}$ that minimizes cR can be found by discrete graphical intervals as shown in Figure 3 or by using a line search. Q_2 is constrained to be unity by performing the minimization of cR for a given ratio, then multiplying both θ and σ_R^2 by Q_2. At the next iteration, Q_2 will be equal to one.

[53] From the optimal set of structural parameters for each zonation candidate, we can evaluate a final metric to guide selection of the best zonation candidate. Relative percent difference (RPD) between cR and the optimal σ_R^2 is

$$RPD = \frac{2\left|cR - \sigma_R^2\right|}{cR + \sigma_R^2} \times 100\% \tag{32}$$

[54] With the constraint of $Q_2 = 1$, cR is equal to the geometric mean of σ^2 noting

$$1 \times \exp\left(\frac{1}{n-p}\sum_{i=p+1}^{n}\ln\left(\sigma_i^2\right)\right) = \left(\prod_{1=p+1}^{n}\sigma_i^2\right)^{\frac{1}{n-p}} \tag{33}$$

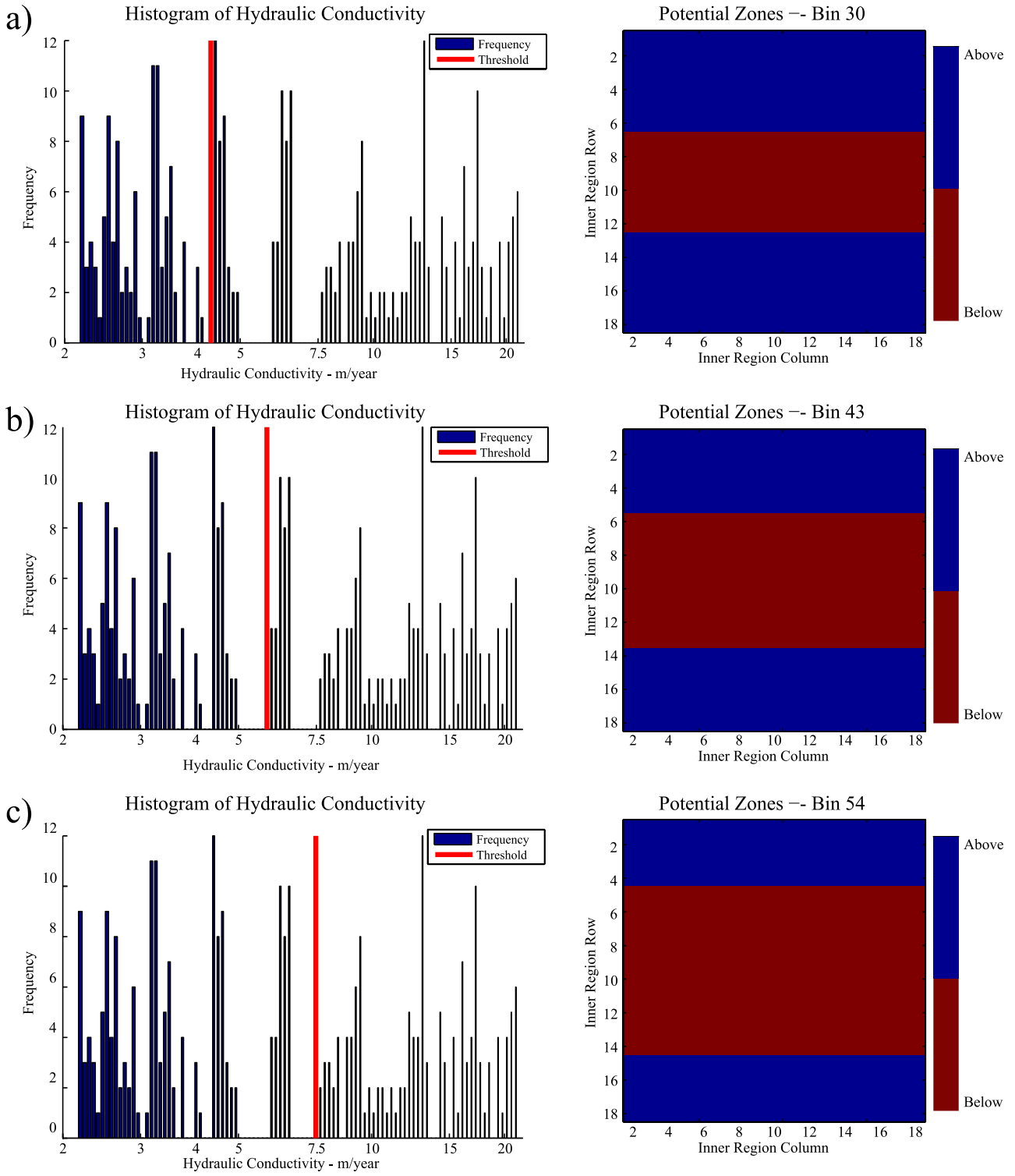

Figure 1. Zone candidates selected from an exponential GCF inversion assuming a single inner region zone for the straight inclusion example. The left plots show histograms of model nodes at each hydraulic conductivity level. The right plots show binary maps of the hydraulic conductivity fields. The gaps were observed at bins 30, 43, and 54.

[55] The RPD metric is therefore a measure of agreement between the epistemic error term (σ_R^2) and the actual error calculated from the orthonormal residuals (cR). In an appropriate model, the epistemic error term (σ_R^2) used in estimation and the error calculated using orthonormal residuals (σ^2) should be close to each other since they are two separate measures of how closely the measurements should agree with the predictions. Selecting the smallest σ_R^2 may lead to selection of an overly rough model that suffers from the problem of overfitting. On the other hand, RPD is

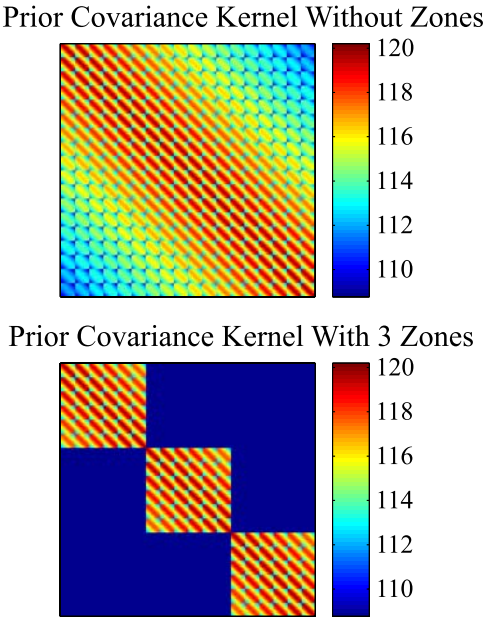

Figure 2. Comparison of the **Q** matrix kernel ($\mathbf{Q_0}$) (top) without zones and (bottom) with zones for an exponential GCF applied to the straight inclusion synthetic example with the lowest-threshold zonation. Note that the lowest values in the bottom plot are equal to zero.

external to the zonation and provides a measure of agreement that is independent of the specific magnitude of residuals. This provides a semiquantitative guide toward selection of an appropriate zonation candidate.

5. Designing a Field Test and Inversion Protocol

[56] The implementation of the methodology outlined above fits into a general protocol based on principles that may be applied to problems regardless of the experimental setup (i.e., SHT or DHT). In either case, N wells are assumed available which can each be configured with a pump or a pressure transducer. This protocol considers steady state pumping tests but transient hydraulic tomography can be performed with minimal modifications to the protocol. The protocol is outlined as follows:

[57] 1. Create a pumping and observation protocol: Whether SHT or DHT will be performed, a systematic scheme of order of pumping the wells and collection of observations in all nonpumped wells is required. For SHT, each of the N wells is pumped individually and pressure is observed in the remaining $N-1$ wells. For DHT, some subset of the $\frac{N(N-1)}{2}$ dipole combinations is pumped while pressure is observed in the remaining $N-2$ wells.

[58] 2. Perform the (steady state) pumping tests: Each pumping test should be performed long enough that steady state is achieved at which point the drawdown in each observation well is recorded. The datum for drawdown in each observation well is the head in that well immediately prior to pumping. At the end of all the tests, a single combined vector of drawdown values, **y**, will serve as the data vector in equation (12) and all subsequent calculations.

[59] 3. Initialize the forward model:

[60] Boundary conditions are set such that stimulations in the core do not impact the boundaries. In this case, constant head boundaries were used.

[61] Initialize the hydraulic conductivity field as $\mathbf{s}_0$. This can be estimated from prior information, assigned as a constant value, or may be a previous estimate from a similar inversion.

[62] Initialize θ and σ_R^2. It is best to start with a high degree of prior information (strong smoothing), i.e., a ratio of $\frac{\theta}{\sigma_R^2}$ less than unity, which makes the solution smooth and stable. Smoothing will be relaxed gradually by increasing the ratio of $\frac{\theta}{\sigma_R^2}$, revealing more structure in the solution until the optimal balance is obtained. This adjustment takes place in step 6.

[63] 4. Run the primary and adjoint problem model runs: The primary model run is a set of forward runs (in this case using MODFLOW) corresponding to each stimulation given the current candidate conductivity field. Initially, the candidate is $\mathbf{s}_0$ and is subsequently referred to as $\tilde{\mathbf{s}}$. The primary model provides the current estimate of the drawdown values, $\mathbf{h}(\tilde{\mathbf{s}})$, which is a vector of the same dimension as **y**. The adjoint problem run calculates the sensitivity matrix $\tilde{\mathbf{H}} = \frac{\partial h(\tilde{\mathbf{s}})_i}{\partial s_j}$. Both results are used to solve equation (15).

[64] 5. Find a new estimate of **s**, referred to as $\hat{\mathbf{s}}$ by solving the following system of equations:

$$\hat{\mathbf{s}} = \mathbf{X}\hat{\beta} + \mathbf{Q}\tilde{\mathbf{H}}^T\xi \tag{34}$$

$$\begin{bmatrix} \boldsymbol{\Sigma} & \tilde{\mathbf{H}}\mathbf{X} \\ (\tilde{\mathbf{H}}\mathbf{X})^{\mathbf{T}} & \mathbf{0} \end{bmatrix} \begin{bmatrix} \xi \\ \hat{\beta} \end{bmatrix} = \begin{bmatrix} \mathbf{y} - \mathbf{h}(\tilde{\mathbf{s}}) + \tilde{\mathbf{H}}\tilde{\mathbf{s}} \\ \mathbf{0} \end{bmatrix} \tag{35}$$

This new estimate ($\hat{\mathbf{s}}$) is compared with the previous estimate ($\tilde{\mathbf{s}}$). These calculations are iterated until $\|\mathcal{L}(\hat{\mathbf{s}}) - \mathcal{L}(\tilde{\mathbf{s}})\|_2$ or $\|\hat{\mathbf{s}} - \tilde{\mathbf{s}}\|_2$ decreases beneath a specified tolerance. A line search may be performed at each iteration to help guide the solution. The line search is beneficial for strongly nonlinear problems, such as those with large contrasts [*Zanini and Kitanidis*, 2008]. For many problems, a line search is not

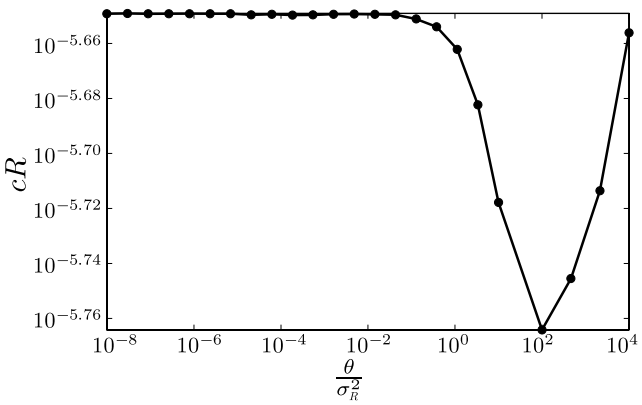

Figure 3. Plot of cR as a function of $\frac{\theta}{\sigma_R^2}$ ratio for the middle zonation example of the straight inclusion synthetic case. The solution with the smallest cR value corresponds to the optimal trade-off between misfit and prior information. In all cases, Q_2 is constrained to unity.

required unless is it established that the solution is stalled and the objective function does not decrease in a satisfactory fashion. An alternative stabilization approach is the modified Levenberg-Marquardt method [*Nowak and Cirpka*, 2004].

[65] 6. Examine the orthonormal residuals to find optimal structural parameters: The entire process, up to this point, proceeds using the initial structural parameter values for **R** and **Q**. To optimize the structural parameters the entire solution to convergence of the objective function ($\|\mathcal{L}(\hat{\mathbf{s}}) - \mathcal{L}(\tilde{\mathbf{s}})\|_2$) and the parameters ($\|\hat{\mathbf{s}} - \tilde{\mathbf{s}}\|_2$) is performed for a range of structural parameters. For each ratio $\frac{\theta}{\sigma_R^2}$, the solution for **s** proceeds to convergence, the metrics Q_2 and cR are calculated, and both structural parameters are multiplied by Q_2, while maintaining their ratio, so that the best estimate stays the same, but the confidence intervals are changed when Q_2 is unity. The ratio with the lowest value of cR is retained as the optimal structural parameter set. When proceeding to the next ratio of $\frac{\theta}{\sigma_R^2}$, use the most recent $\hat{\mathbf{s}}$ as the starting value. It should be closer to the true **s** than a totally uniform guess and will speed convergence.

[66] 7. Explore zonation candidates: Use the zonation approach outlined in section 3.2.2.1 above to select several candidates for zonation. For each candidate, perform the entire inversion (steps 4–6).

[67] 8. Evaluate the best zonation candidate: Three metrics guide which zonation candidate is best. The cR (equation (31)) value should be low, with Q_2 (equation (30)) constrained to be one and the relative percent difference (RPD) between cR and σ_R^2 should be low (equation (32)).

6. Sensitivity Matrices and Splines

[68] *Kitanidis* [1998] and Snodgrass and *Kitanidis* [1998] discussed the use of sensitivity matrices and interpolation splines to examine the behavior of geostatistical inversion. The solution for the best estimate from equation (17) at each parameter node location is the superposition of a mean value ($\mathbf{X}\hat{\beta}$) and an interpolation "spline" ($\mathbf{QH}^T$) weighted by ξ. The matrix **X** associates the node location with the appropriate mean value of $\hat{\beta}$ which is estimated by solving the system in equation (18) or equation (20). The interpolation weights, ξ, are calculated in the same system and are used, combined with the data-model cross covariance ($\mathbf{QH}^T$) to map the influence of each observation in **y** to the parameters. To understand both the influence of specific measurements in **y** on the best estimate, and to see which nodes are expected to be estimable, we can inspect both the raw sensitivity (**H**) and the splines ($\mathbf{QH}^T$). This discussion is in the context of the specific model presented in section 7. The examination of sensitivity and splines can guide the selection of both well configurations and pumping strategies.

[69] The row of the sensitivity matrix (**H**) corresponding to an individual measurement can be projected onto the conductivity field, which is done for each observation for the DHT protocol in Figure 4. In Figure 4, the color scale is truncated to show detail of the field away from the well locations which would otherwise be eclipsed by very few very high values immediately adjacent to the pumping and observations wells. For comparability, the reference K field is a homogeneous field with magnitude equal to the mean of the true solution. A homogeneous reference field was selected because it highlights sensitivity resulting from well arrangement and protocol rather than K contrasts.

[70] The "splines" incorporate information from the prior covariance matrix **Q**. Particularly in the case of a linear prior covariance model, this information is diffuse and both stabilizes the solution and enforces smoothness in the best estimate and realizations. Figure 5 shows the normalized splines projected onto the computational domain. The normalization is performed relative to the highest value in the specific column of $\mathbf{QH}^T$ and reveals the general shape of the splines throughout the domain. The splines and sensitivities with the greatest contribution are those in which the injection and extraction wells span the domain and the observation well is near one of the pumped wells. Examples are R 4/Ob 1 and R 12/Ob 4 in Figure 5. The sign of both the sensitivity and the spline is controlled by proximity of the observation well to a pumped well. Negative sensitivity coefficients occur near extraction wells whereas positive sensitivity coefficients occur near injection wells. The least sensitive configurations are those when the dipole is induced entirely along one edge of the domain at two corners and the observation well is either between or on the center of the opposite edge. The observations for Runs 2 and 14 illustrate these configurations. When the dipole is induced at two opposite corners with the observation well in a third corner, sensitivity is also very diffuse and the splines not very informative. The result is that the greatest sensitivity and, correspondingly, the most informative splines occur along the centerline of the K field. Interrogation of the corners of the K field is weaker using dipoles, and in general, significant spread is observed through the field.

7. Illustrative Examples

[71] We present three examples to illustrate the protocol outlined above. They are synthetic examples chosen to challenge the applicability of the method, particularly the chosen generalized covariance function (GCF). The linear GCF gives best results when applied to continuously varying fields. However, it is a flexible GCF and often serves as the first choice in inverse problems when little is known about the structure of parameter space. Applying this model to a parameter field with strong discontinuities highlights its flexibility but also pushes it to its limit of applicability. Implementation is performed using a special exponential GCF discussed in section 3.2.1 to approximate the linear. Discussion of the use of sensitivity matrices and splines was presented in the context of these specific examples.

[72] In each example, the core is surrounded by a buffer zone with $K = 50\frac{m}{year}$. The buffer zone extends nearly 1 km in each direction and ensures that the boundary conditions do not play a role in the tests. In the stationary heterogeneous example, K ranges from 1 to $12\frac{m}{year}$ whereas the inclusion examples contain an inclusion with $K = 1\frac{m}{year}$ surrounded by a $K = 10\frac{m}{year}$ matrix. The aquifer is modeled as confined and two dimensional, with observations recorded at steady state. The inner region for all three examples is 9×9 meters with square discretization and $0.5m$ nodes resulting in 324 K values to estimate as shown in Figure 6. No wells are included within the inner region but six wells are included along the edges. No recharge is

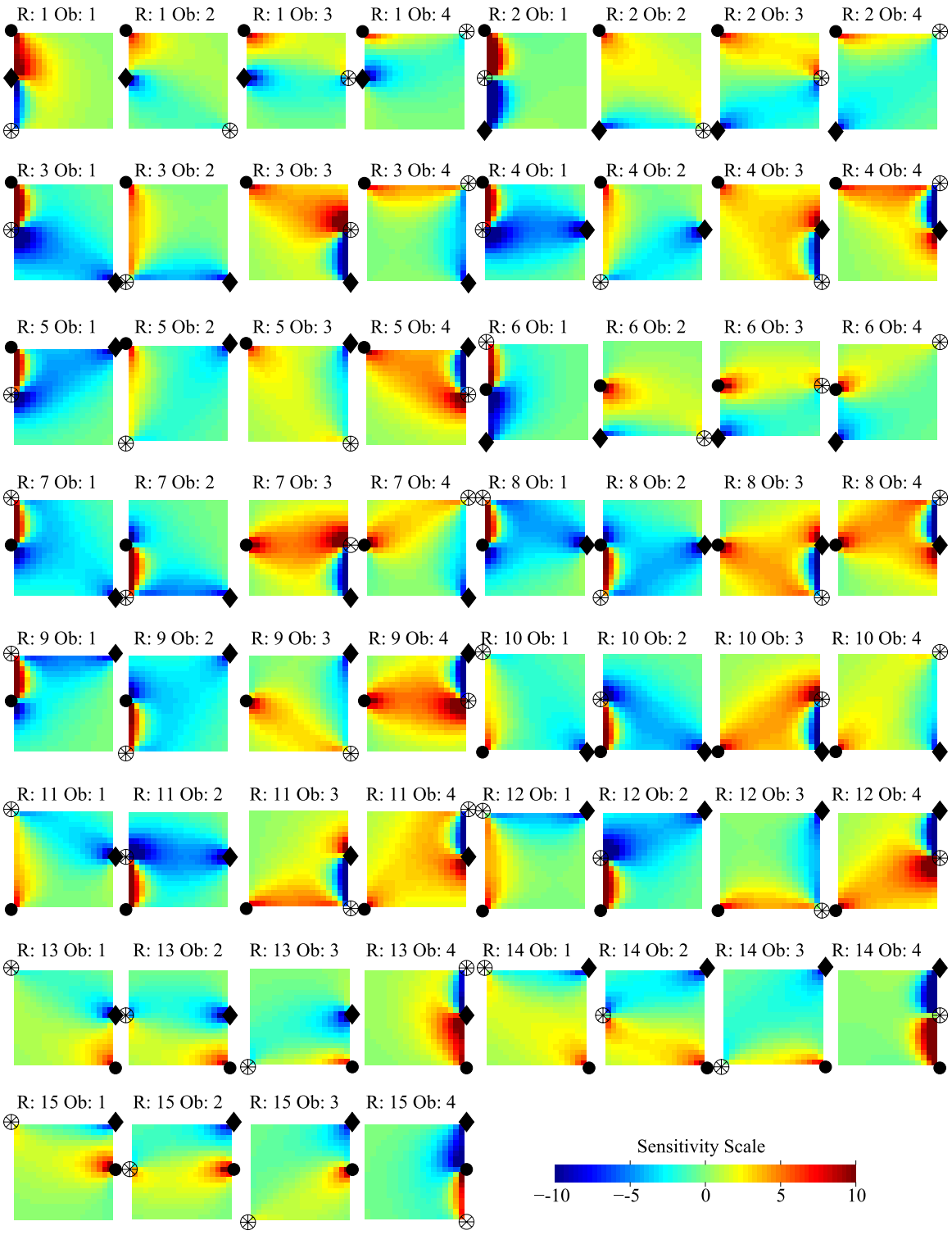

Figure 4. Sensitivity matrix **H** for DHT observations assuming a homogeneous K field. The n rows of **H** are displayed on n plots, mapped onto the geometry of the inner region model nodes. Solid circles are extraction wells, solid diamonds are injection wells, and circled asterisks are observation wells. The scale is truncated at the high and low ends to show detail in the middle; actual values immediately adjacent to wells are more extreme than −10 to 10. In each title, "R" refers to the dipole test number, and "Ob" refers to the observation number. For this problem with six wells, 15 dipole tests are performed, each with four observations.

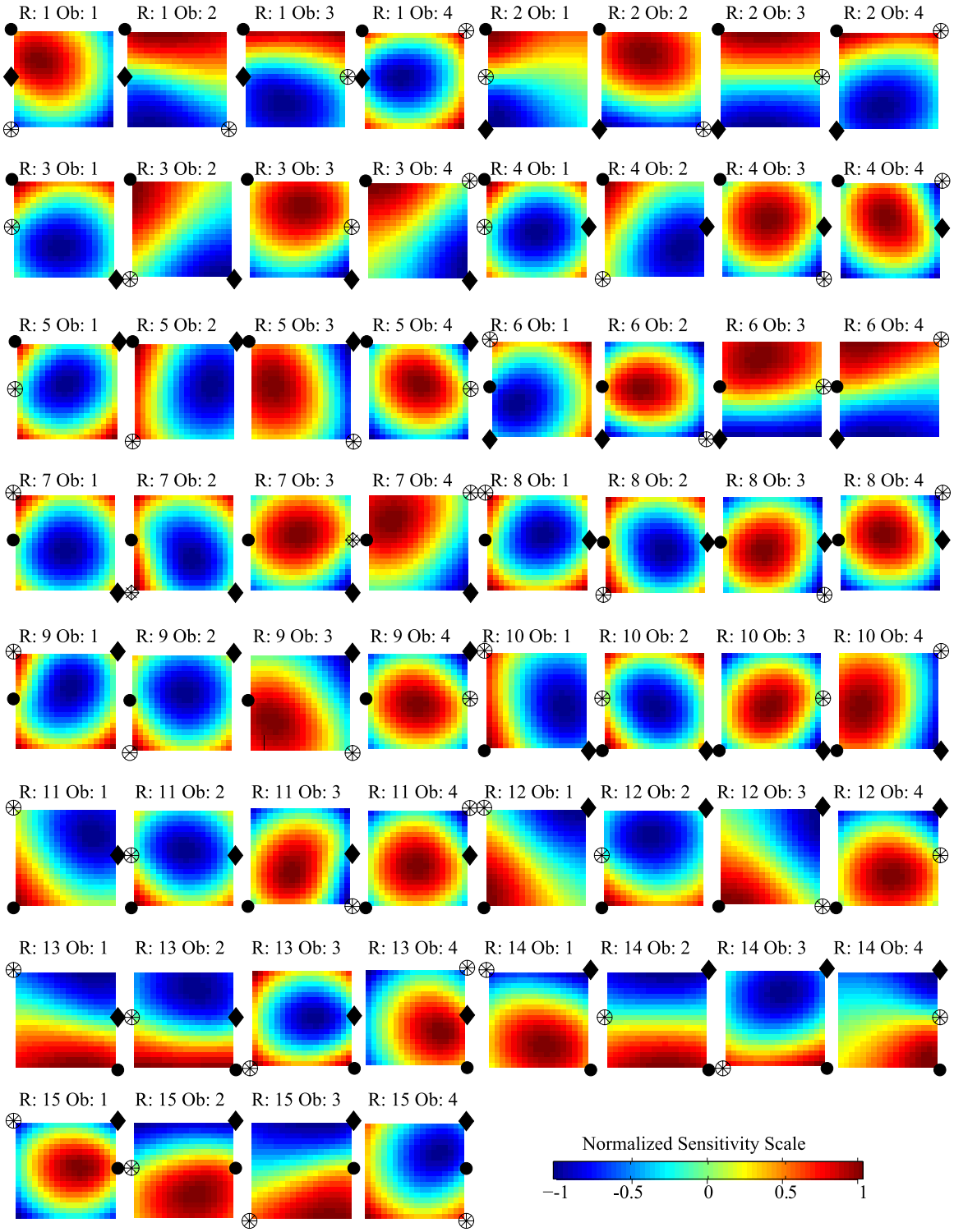

Figure 5. Interpolation splines for DHT displayed on the inner region model nodes. Reference K field and legend are the same as in Figure 4. Scale is normalized to largest value in each plot to reveal internal structure.

applied so the only sources of water is inflow from the distant boundaries at which constant head is enforced, and injection in wells in the dipole case. In the case of dipoles, the injection well is the source of water extracted from the extraction well and the head field is not perturbed very far from the core. As discussed above, the changes in head due to pumping (drawdowns) are used. The entire buffer has a single constant value which is unknown a priori and is estimated along with the inner region. As a result, the **Q**, **H**, and **X** matrices account for a homogeneous zone that contains all nodes in the buffer zone.

[73] As synthetic examples, the forward model must be run using the true K field to obtain the measurements (**y**). These measurements are corrupted with a small, normally

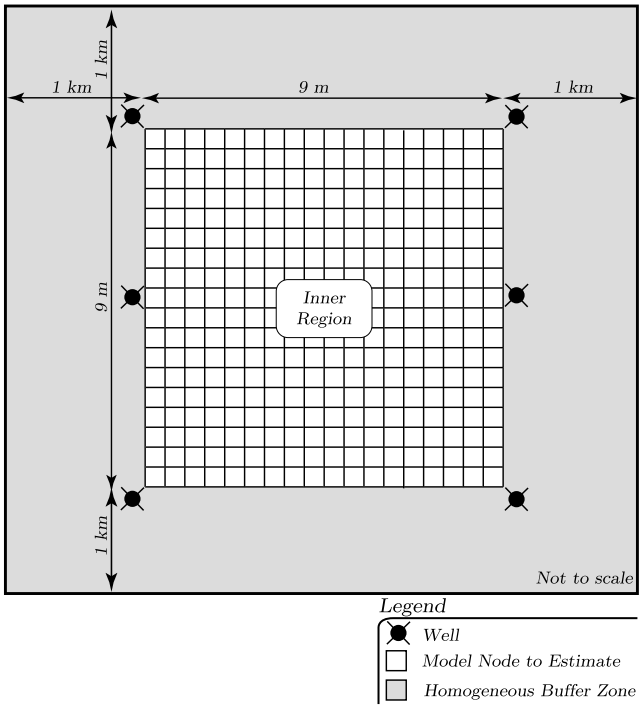

Figure 6. Overview of the model domain showing wells and nodes. Each well can be either pumped or used for observation, according to the protocol of the particular stimulation. The inner region is surrounded by a homogeneous buffer extending 1 km in each direction, depicted in gray, intended to attenuate the impact of boundary conditions.

distributed noise ($N\tilde{}(0, 1 \times 10^{-4})$) to represent measurement uncertainty before being used in the inverse solution. To start the estimation, the algorithm is seeded with a constant value (the overall mean of the K field).

[74] All examples were analyzed using both DHT and SHT protocols but only DHT results are discussed in this work. *Fienen* [2007] gives an expanded discussion of SHT protocol results. SHT results were generally comparable although in several cases the impact of measurement noise was much more significant than in the DHT results.

[75] For the DHT protocol, each dipole configuration is used resulting in 15 stimulation events, each with 4 observations yielding 60 discrete drawdown observations. For each dipole, one well extracts and the other injects at 95 liters per minute. In dipoles of unequal strength, the results of which well is injection and which is extraction

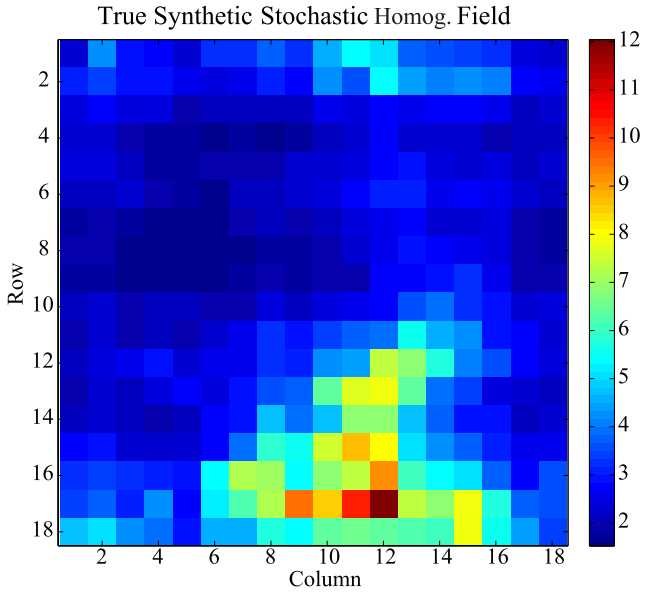

Figure 7. True hydraulic conductivity (K) field for the stationary heterogeneous field synthetic example.

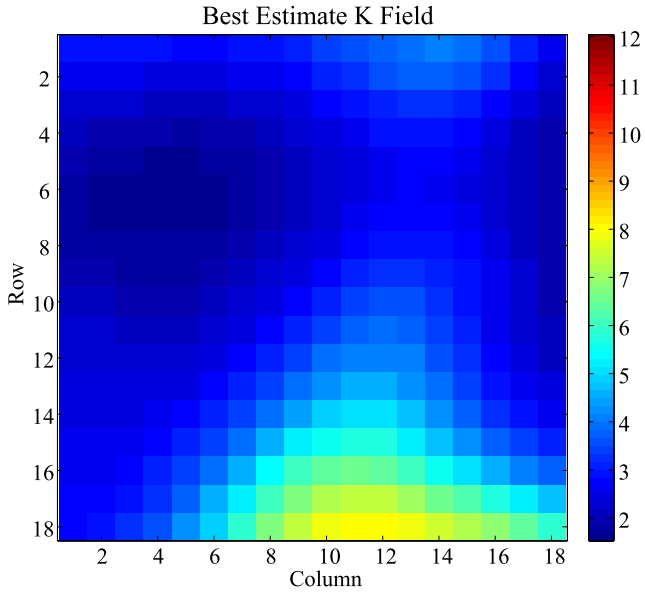

Figure 8. Best estimate of the K field for the stationary heterogeneous field synthetic example.

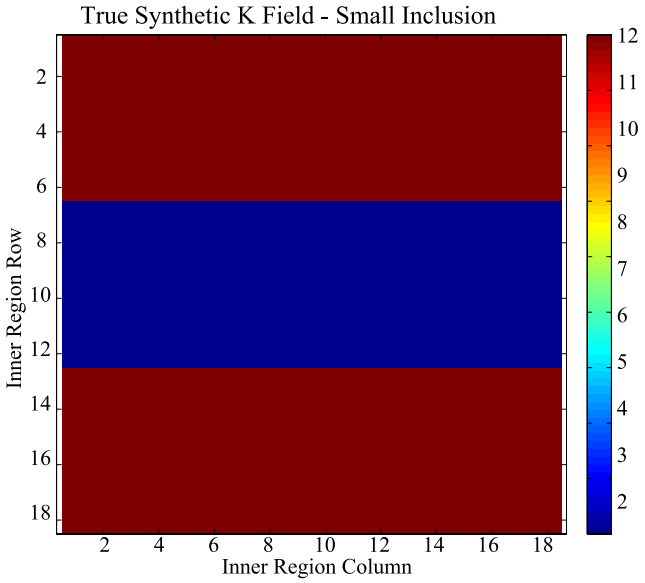

Figure 9. True hydraulic conductivity (K) field for the straight inclusion synthetic example.

interrogate different areas in the aquifer and provide different information to the inversion. Therefore, in such cases, it is advantageous to pump each dipole twice; once for each configuration. In this case, however, the dipoles are of equal strength, so each pair is pumped only once. The results of all dipoles are calibrated simultaneously.

[76] The protocol outlined above is then applied to estimate structural parameters and evaluate zonation strategies.

7.1. Stationary Heterogeneous Field Example

[77] The first example is a smoothly varying synthetic field shown in Figure 7. This represents a mildly heterogeneous field and should be easy to find with this method without any zonation. Figure 8 shows the best estimate of the hydraulic conductivity field. The result is smoother than the true solution with the major features well represented. Applying the principle of parsimony, one could argue that an estimation grid of four or five homogeneous zones could represent this field nearly as well as this highly parameterized solution. However, it would be impossible to know a priori where to draw the boundaries of the homogeneous zones. The flexibility of this method allowed the data to indicate the appropriate level of smoothness that could capture the variability due to optimal calculation of the structural parameters.

[78] This finding is possible chiefly because there are no significant discontinuities that the prior GCF must handle. This example proves that when the structure conforms to the model of stationarity and spatial continuity, the algorithm performs very well. The remaining two examples are less ideal and both contain significant discontinuities that force us to seek and employ zones with independent means.

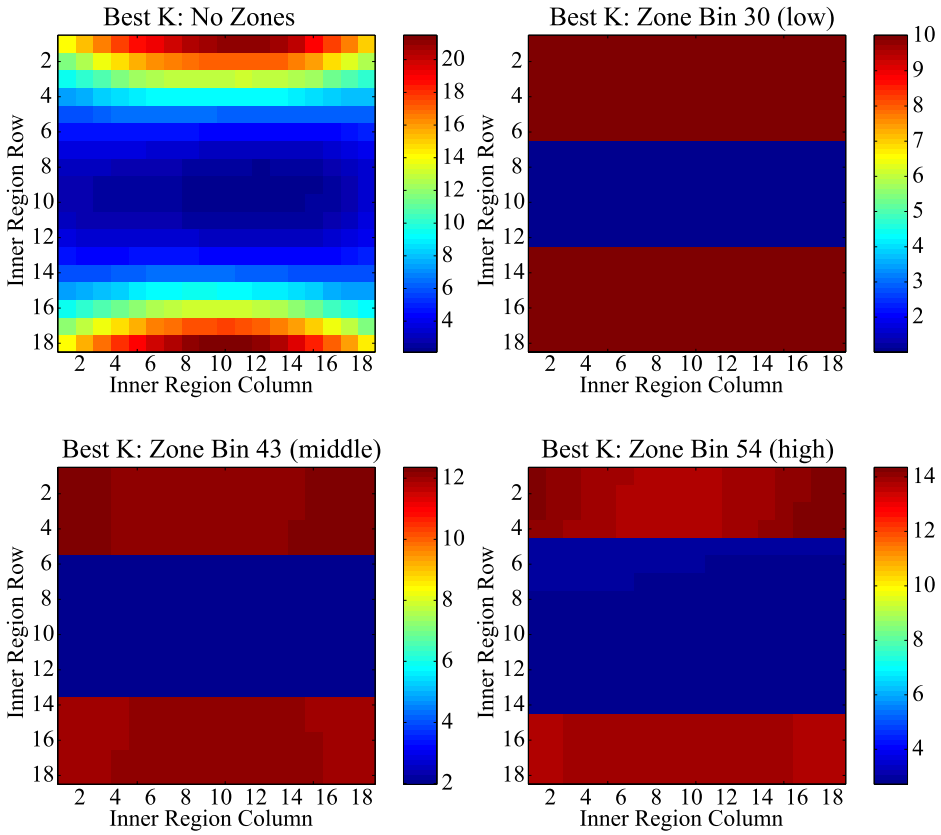

Figure 10. Best estimates for the straight inclusion synthetic example: (top left) no zones, (top right) low-zone candidate, (bottom left) middle-zone candidate, and (bottom right) high-zone candidate. The scales are different in each plot to reveal structure.

Table 1. Structural Parameter Metrics Values for Several Zonation Schemes in the Straight Inclusion Synthetic Example for DHT

Parameter	No Zones	Low Threshold	Middle Threshold	High Threshold
cR	5.70×10^{-6}	1.00×10^{-6}	1.72×10^{-6}	2.33×10^{-6}
Optimal σ_R^2	1.44×10^{-6}	1.19×10^{-6}	1.42×10^{-6}	1.78×10^{-6}
RPD, %	120	18	19	27
MSE	19.42	1.91×10^{-4}	9.91	19.31

7.2. Straight Inclusion Example

[79] The second example is a straight inclusion shown in Figure 9. Low hydraulic conductivity inclusions in a higher-conductivity matrix may occur in a fluvial environment where the matrix is typical river sands and gravels while the lower-conductivity inclusion is the remnant of a point bar deposit or overbank deposit made up of finer-grained material. The first inversion was performed without using zonation and the best estimate is shown in the upper left panel of Figure 10. The general pattern is reasonable with the boundaries between the lower-K inclusion and the surrounding matrix in the right location. However, the higher-K regions at the upper and lower portions of the inner region are artificially smooth and overshoot the higher K values as the selected GCF is ill suited to represent discontinuities. Figure 1 shows three candidate zonation approaches based on the first three significant gaps in the histogram of K. The results of the three zonation candidates are shown in Figure 10. The lowest-zonation candidate in the upper right panels of Figure 10 perfectly represents the geometry of the true K regions. The resulting solutions are nearly perfect as well since the GCF does not need to account for the discontinuity. The structural parameter metrics are outlined in Table 1. The RPD (equation (32)) is lowest for the low-zonation candidate in this case. This is also indicated to be best by the mean square error for the hydraulic conductivity field (MSE) calculated as

$$\frac{\sum_{i=1}^{m} (K_{est} - K_{true})^2}{m} \tag{36}$$

where K_{est} and K_{true} are the estimated and actual parameter values in each of the m model nodes of the inner region.

[80] This calculation is only possible for synthetic cases, of course. The ability to compare the results among zonation candidates to "truth" is an advantage of evaluating the method using a synthetic example.

7.3. Angled Inclusion Example

[81] The third example, depicted in Figure 11, is a narrow inclusion at an angle oblique to the principal directions of the model domain which could indicate a clay lens. Three zonation candidates were chosen on the basis of the histograms presented in Figure 12. The gaps are not as clearly defined as in the straight inclusion example. The lowest gap was initially selected, but the inclusion was implied to be too small and the imposition of such an erroneous zonation scheme was unstable precluding a meaningful inversion. The process of selection and evaluation of the zones is subject not only to the metrics presented in this work, but also judgment of the practitioner.

[82] As with the previous example, the general shape of the inclusion is found with DHT even without zones as shown in Figure 13. Remarkably, the angle of the inclusion is well represented in the solution and the general extent is reasonable with some smearing. The lowest of the selected histogram gaps yields the closest solution as indicated by the MSE value reported on Table 2. The associated RPD (equation (32)) values indicate that zones should provide better results than a nonzoned approach, but do not distinguish particularly well among the zonation candidates.

8. Conclusions

[83] This work presents an interactive protocol for hydraulic tomography using the Bayesian geostatistical inverse method. The interactive aspects of the protocol allow the imposition of expert judgment and allow practitioners to investigate the ramifications of their choices. The metrics from orthonormal residuals provide important guidance regarding selection of zones and smoothing versus data reproduction. However, it is up to practitioners to evaluate the geologic realism provided in each solution. In the determination of structural parameters and, to a greater extent, in the selection of zones, interactive opportunities allow practitioners to audit to algorithm and override "decisions" indicated by the metrics available. Inverse modeling is not a black box, and expert knowledge still plays an important role in obtaining realistic and meaningful estimates of hydrogeologic parameters.

[84] The Bayesian method explicitly considers epistemic uncertainty and imposes a minimum of prior assumptions on the parameters. We showed that favorable results can be

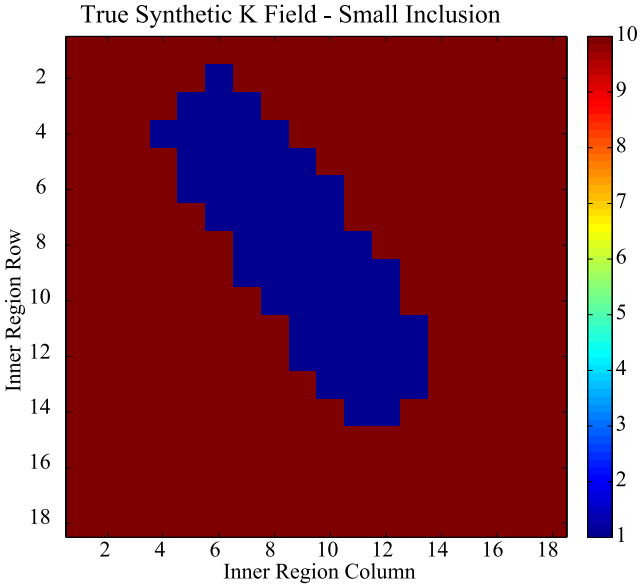

Figure 11. True hydraulic conductivity (K) field for the angled inclusion synthetic example.

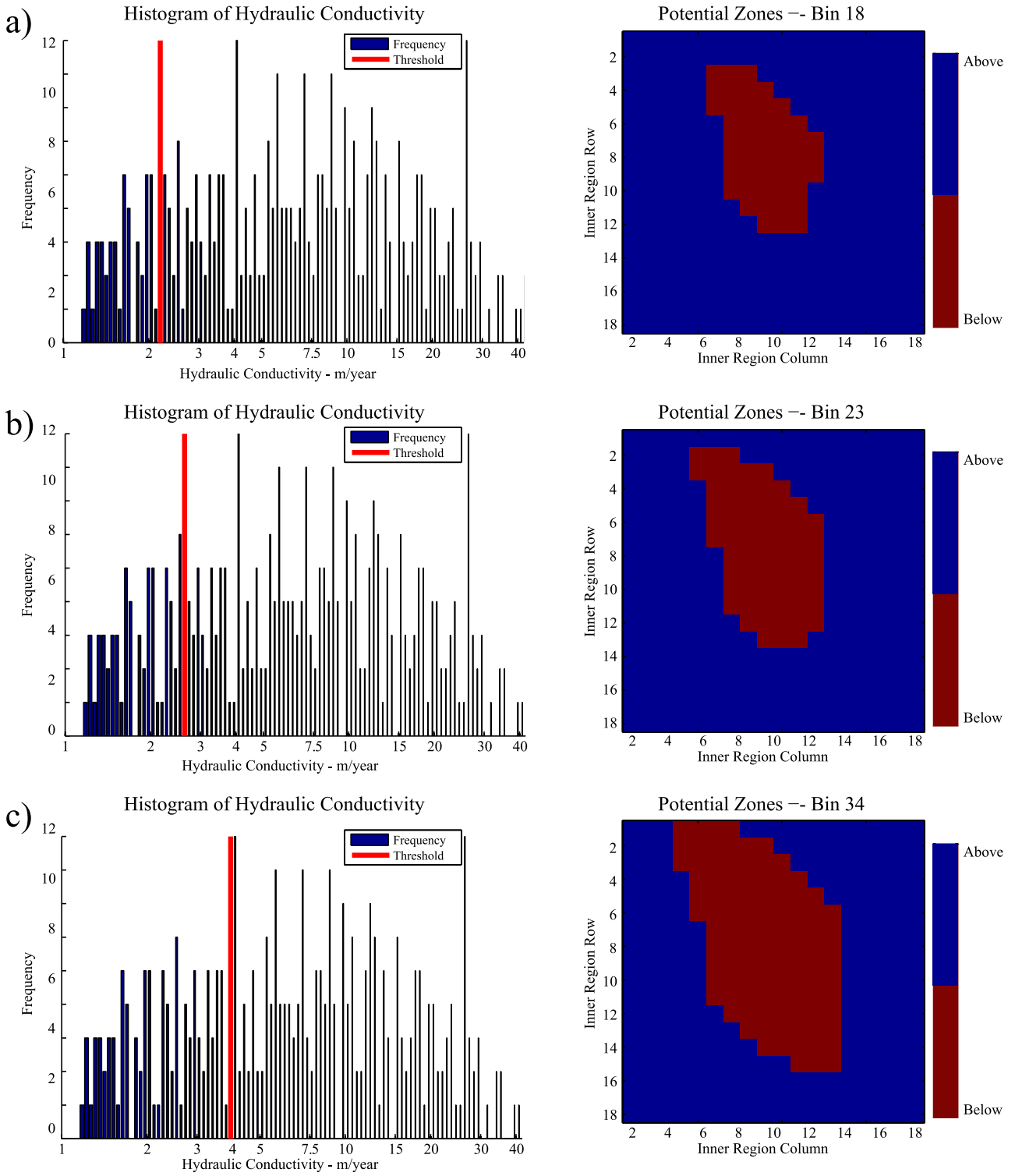

Figure 12. Zone candidates selected from an exponential GCF inversion assuming a single inner region zone for the angled inclusion example. The left plots show histograms of pixels at each hydraulic conductivity level. The right plots show binary maps of the hydraulic conductivity fields. The gaps were observed at bins 18, 23, and 34.

obtained with a relatively small number of wells, even if located entirely outside the domain in which hydraulic conductivity parameters are estimated. This could be the field setup in a case of limited access when seeking lateral extent information, or a series of cross-sectional multilevel screened wells in a cross-hole context analogous to seismic or electrical resistivity tomography. In the cross-sectional case, a three-dimensional model may be more appropriate. However, our method is not limited to cases where all wells are outside the domain of interest. In many cases, wells are

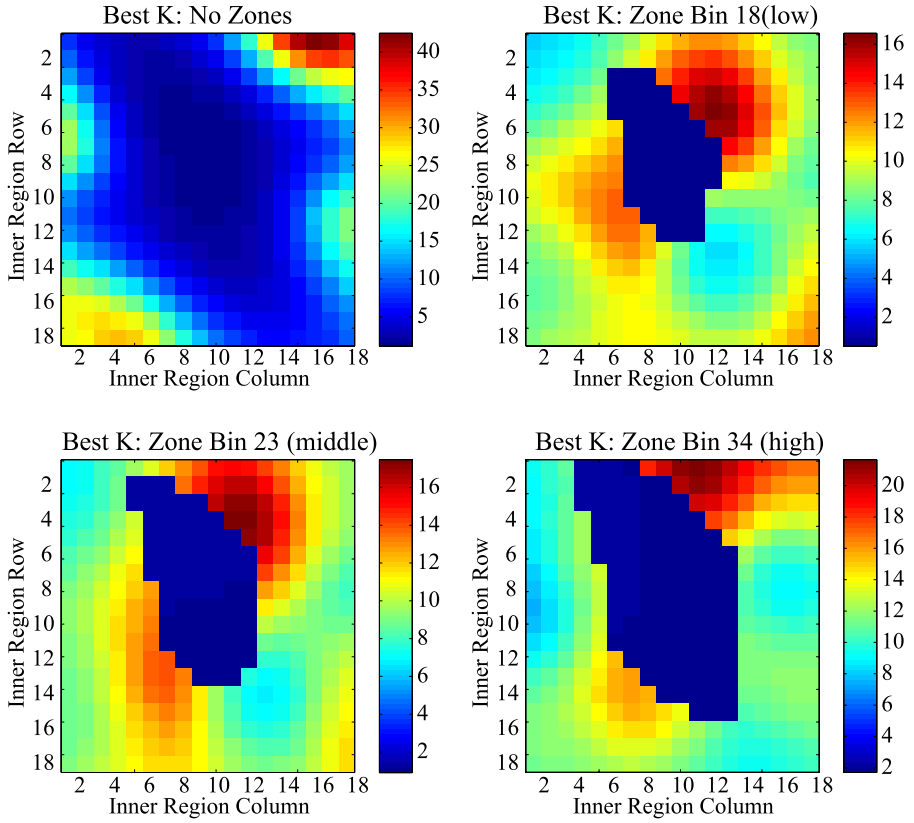

Figure 13. Best estimates for the angled inclusion synthetic example: (top left) no zones, (top right) low-zone candidate, (bottom left) middle-zone candidate, and (bottom right) high-zone candidate. The scales are different in each plot to reveal structure within each solution.

available within the domain of interest and these wells may be extremely valuable, providing significant information about the parameters. An important source of uncertainty is alleviated in this protocol by referencing all head measurements to immediately antecedent levels. Using drawdown mitigates the impact that longer-term variations in regional conditions could otherwise have on confounding the parameter estimation over the relatively short duration of each hydraulic tomography stimulation event.

[85] The adjoint state implementation is an efficient and accurate means to calculate the sensitivities. Examination of sensitivities and interpolation splines provides valuable information about which well configurations provide the most information about the parameter field. Particularly in the case of dipole hydraulic tomography, this information can guide the selection of a subset of dipoles from an existing well field to incorporate into a hydraulic tomography experiment.

[86] The examination of orthonormal residuals proved to be an effective tool in evaluating the trade-off between data reproduction and prior information. The cR and Q_2 metrics were supplemented by a new metric, the RPD, which is the relative percent difference between the optimal epistemic error parameter (σ_R^2) and cR, interpreted as a proxy for σ_R^2 measured from a given solution. The RPD should be low when these values are in agreement and it was shown to provide guidance about when to accept candidate models (on the basis of zonation choices) to improve the best estimate results.

[87] Zonation was shown to be a powerful force in obtaining best estimates for problems of low-K inclusions. The best estimate of the K field obtained without zones resulted in oversmoothing where the prior covariance model was taxed too much trying to capture discontinuities in the field. Zones determined through active examination of preliminary nonzoned results yielded excellent solutions, particularly when the zone choices closely matched the inclusion dimensions. When the zones were selected inappropriately, the solution suffered, but the metrics used here provided guidance on which to accept and which to reject.

Table 2. Structural Parameter Metrics Values for Several Zonation Schemes in the Angled Inclusion Synthetic Example for DHT

Parameter	No Zones	Low Threshold	Middle Threshold	High Threshold
cR	7.66×10^{-6}	4.38×10^{-6}	4.37×10^{-6}	4.16×10^{-6}
Optimal σ_R^2	1.24×10^{-6}	1.38×10^{-6}	1.50×10^{-6}	1.32×10^{-6}
RPD, %	144	104	98	104
MSE	60.77	9.44	10.84	19.59

The promise shown by a combination of the linear prior covariance model and zones motivates future development of more robust zonation strategies.

[88] **Acknowledgments.** The authors wish to acknowledge critical reviews by Michael Cardiff, Randy Hunt, Wolfgang Nowak, Scott Tyler, Alberto Montanari, Mary Hill, and two anonymous reviewers, all of which greatly improved this manuscript. This work was funded by the Office of Biological and Environmental Research (BER) Environmental Remediation Sciences Program (ERSP); U.S. Department of Energy (DOE) under grant number DOEAC05-00OR22725; the National Research Council Postdoctoral Research Associateship program; the USGS Trout Lake Water, Energy, and Biogeochemical Budgets (WEBB) project; and the USGS Office of Groundwater. Development of the code for adjoint state sensitivities in MODFLOW was supported by Army Research Office grants DAAH04-96-1-0318 and DAAD19-00-1-0454 and U.S. Environmental Protection Agency grant X-970085-01-0.

References

Batu, V. (1998), *Aquifer Hydraulics: A Comprehensive Guide to Hydrogeologic Data Analysis*, John Wiley, New York.

Bohling, G. C. (1993), Hydraulic tomography in two-dimensional, steady-state groundwater flow, *Eos Trans. AGU*, *74*(16), Spring Meet. Suppl., 141.

Bohling, G. C., X. Zhan, J. J. Butler Jr., and L. Zheng (2002), Steady shape analysis of tomographic pumping tests for characterization of aquifer heterogeneities, *Water Resour. Res.*, *38*(12), 1324, doi:10.1029/2001WR001176.

Bohling, G. C., J. J. Butler Jr., X. Zhan, and M. D. Knoll (2007), A field assessment of the value of steady shape hydraulic tomography for characterization of aquifer heterogeneities, *Water Resour. Res.*, *43*, W05430, doi:10.1029/2006WR004932.

Brauchler, R. (2005), Characterization of fractured porous media using multivariate statistics and hydraulic travel time tomography, Ph.D. dissertation, Univ. Tübingen, Tübingen, Germany.

Butler, J. J., Jr., C. D. McElwee, and G. C. Bohling (1999), Pumping tests in networks of multilevel sampling wells: Motivation and methodology, *Water Resour. Res.*, *35*(11), 3553–3560, doi:10.1029/1999WR900231.

Caers, J., and T. Zhang (2004), Multiple-point geostatistics: A quantitative vehicle for integrating geologic analogs into multiple reservoir models, in *Integration of Outcrop and Modern Analogs in Reservoir Modeling*, edited by G. M. Grammer, P. M. Harris, and G. P. Eberli, *AAPG Mem.*, *80*, 383–394.

Clemo, T. (2007), MODFLOW-2005 ground water model—User guide to the adjoint state based sensitivity process (ADJ), *Tech. Rep. BSU CGISS 07-01*, Boise State Univ., Boise, Idaho.

Fetter, C. (1994), *Applied Hydrogeology*, 3rd ed., Prentice-Hall, Upper Saddle River, N. J.

Feyen, L., and J. Caers (2006), Quantifying geological uncertainty for flow and transport modeling in multi-modal heterogeneous formations, *Adv. Water Resour.*, *29*(6), 912–929, doi:10.1016/j.advwatres.2005.08.002.

Fienen, M. N. (2007), Inverse methods for nearfield hydrogeologic characterization, Ph.D. dissertation, Stanford Univ., Stanford, Calif.

Fienen, M. N., P. K. Kitanidis, D. Watson, and P. Jardine (2004), An application of Bayesian inverse methods to vertical deconvolution of hydraulic conductivity in a heterogeneous aquifer at Oak Ridge National Laboratory, *Math. Geol.*, *36*(1), 101–126, doi:10.1023/B:MATG.0000016232.71993.bd.

Fienen, M. N., J. Luo, and P. K. Kitanidis (2006), A Bayesian geostatistical transfer function approach to tracer test analysis, *Water Resour. Res.*, *42*, W07426, doi:10.1029/2005WR004576.

Freyberg, D. L. (1986), A natural gradient experiment on solute transport in a sand aquifer: 2. Spatial moments and the advection and dispersion of nonreactive tracers, *Water Resour. Res.*, *22*(13), 2031–2046, doi:10.1029/WR022i013p02031.

Gaganis, P., and L. Smith (2001), A Bayesian approach to the quantification of the effect of model error on the predictions of groundwater models, *Water Resour. Res.*, *37*(9), 2309–2322, doi:10.1029/2000WR000001.

Gallagher, M. R., and J. Doherty (2007), Parameter interdependence and uncertainty induced by lumping in a hydrologic model, *Water Resour. Res.*, *43*, W05421, doi:10.1029/2006WR005347.

Giudici, M., G. Morossi, G. Parravicini, and G. Ponzini (1995), A new method for the identification of distributed transmissivities, *Water Resour. Res.*, *31*(8), 1969–1988, doi:10.1029/95WR01205.

Gottlieb, J., and P. Dietrich (1995), Identification of the permeability distribution in soil by hydraulic tomography, *Inverse Probl.*, *11*(2), 353–360, doi:10.1088/0266-5611/11/2/005.

Harbaugh, A. W., E. W. Banta, M. Hill, and M. G. McDonald (2000), MODFLOW-2000, the U.S. Geological Survey modular ground-water model—User guide to modularization concepts and the ground-water flow process, *U. S. Geol. Surv. Open File Rep.*, *00-92*.

Hoeksema, R. J., and P. K. Kitanidis (1984), An application of the geostatistical approach to the inverse problem in two-dimensional groundwater modeling, *Water Resour. Res.*, *20*(7), 1003–1020, doi:10.1029/WR020i007p01003.

Hyndman, D. W., J. M. Harris, and S. M. Gorelick (2000), Inferring the relation between seismic slowness and hydraulic conductivity in heterogeneous aquifers, *Water Resour. Res.*, *36*(8), 2121–2132, doi:10.1029/2000WR900112.

Illman, W. A., X. Liu, and A. Craig (2007), Steady-state hydraulic tomography in a laboratory aquifer with deterministic heterogeneity: Multimethod and multiscale validation of hydraulic conductivity tomograms, *J. Hydrol.*, *341*(3–4), 222–234, doi:10.1016/j.jhydrol.2007.05.011.

Journel, A. G. (1983), Nonparametric estimation of spatial distributions, *Math. Geol.*, *15*(3), 445–468, doi:10.1007/BF01031292.

Kitanidis, P. K. (1991), Orthonormal residuals in geostatistics: Model criticism and parameter estimation, *Math. Geol.*, *23*(5), 741–758, doi:10.1007/BF02082534.

Kitanidis, P. K. (1995), Quasi-linear geostatistical theory for inversing, *Water Resour. Res.*, *31*(10), 2411–2419, doi:10.1029/95WR01945.

Kitanidis, P. K. (1997), *Introduction to Geostatistics: Applications in Hydrogeology*, Cambridge Univ. Press, New York.

Kitanidis, P. K. (1998), How observations and structure affect the geostatistical solution to the steady-state inverse problem, *Ground Water*, *36*(5), 754–763, doi:10.1111/j.1745-6584.1998.tb02192.x.

Kruseman, G. P., and N. A. De Ridder (1990), *Analysis and Evaluation of Pumping Test Data*, 2nd ed., Int. Inst. for Land Reclam. and Impr., Wageningen, Netherlands.

Kunstmann, H., W. Kinzelbach, P. Marschall, and G. Li (1997), Joint inversion of tracer tests using reversed flow fields, *J. Contam. Hydrol.*, *26*(1–4), 215–226, doi:10.1016/S0169-7722(96)00070-8.

Li, W., and O. A. Cirpka (2006), Efficient geostatistical inverse methods for structured and unstructured grids, *Water Resour. Res.*, *42*, W06402, doi:10.1029/2005WR004668.

Li, W., W. Nowak, and O. A. Cirpka (2005), Geostatistical inverse modeling of transient pumping tests using temporal moments of drawdown, *Water Resour. Res.*, *41*, W08403, doi:10.1029/2004WR003874.

Li, W., A. Englert, O. A. Cirpka, J. Vanderborght, and H. Vereecken (2007), Two-dimensional characterization of hydraulic heterogeneity by multiple pumping tests, *Water Resour. Res.*, *43*, W04433, doi:10.1029/2006WR005333.

Liu, S., T.-C. J. Yeh, and R. Gardiner (2002), Effectiveness of hydraulic tomography: Sandbox experiments, *Water Resour. Res.*, *38*(4), 1034, doi:10.1029/2001WR000338.

Liu, X., W. A. Illman, A. J. Craig, J. Zhu, and T.-C. J. Yeh (2007), Laboratory sandbox validation of transient hydraulic tomography, *Water Resour. Res.*, *43*, W05404, doi:10.1029/2006WR005144.

Mackay, D. M., D. L. Freyberg, P. V. Roberts, and J. A. Cherry (1986), A natural gradient experiment on solute transport in a sand aquifer: 1. Approach and overview of plume movement, *Water Resour. Res.*, *22*(13), 2017–2029, doi:10.1029/WR022i013p02017.

Michalak, A. M., and P. K. Kitanidis (2003), A method for enforcing parameter nonnegativity in Bayesian inverse problems with an application to contaminant source identification, *Water Resour. Res.*, *39*(2), 1033, doi:10.1029/2002WR001480.

Nowak, W., and O. A. Cirpka (2004), A modified Levenberg-Marquardt algorithm for quasi-linear geostatistical inversing, *Adv. Water Resour.*, *27*(7), 737–750, doi:10.1016/j.advwatres.2004.03.004.

Oliver, D. S., and S. Aramco (1990), The averaging process in permeability estimation from well-test data, *SPE Form. Eval.*, *5*(3), 319–324, doi:10.2118/19845-PA.

Portniaguine, O., and M. S. Zhdanov (1999), Focusing geophysical inversion images, *Geophysics*, *64*(3), 874–887, doi:10.1190/1.1444596.

Portniaguine, O., and M. S. Zhdanov (2002), 3-D magnetic inversion with data compression and image focusing, *Geophysics*, *67*(5), 1532–1541, doi:10.1190/1.1512749.

Sharma, P. V. (1997), *Environmental and Engineering Geophysics*, Cambridge Univ. Press, Cambridge, U. K.

Slichter, C. S. (1899), Theoretical investigation of the motion of ground waters, in *19th Annual Report of the U.S. Geological Survey, Part II*, pp. 295–384, Washington, D. C.

Snodgrass, M. F., and P. K. Kitanidis (1998), Transmissivity identification through multi-directional aquifer stimulation, *Stochastic Hydrol. Hydraul.*, *12*(5), 299–316, doi:10.1007/s004770050023.

Straface, S., T.-C. J. Yeh, J. Zhu, S. Troisi, and C. H. Lee (2007), Sequential aquifer tests at a well field, Montalto Uffugo Scalo, Italy, *Water Resour. Res.*, *43*, W07432, doi:10.1029/2006WR005287.

Sun, N.-Z. (1994), *Inverse Problems in Groundwater Modeling*, *Theor. Appl. Transp. Porous Media*, vol. 6, Kluwer Acad., Dordrecht, Netherlands.

Sykes, J. F., J. L. Wilson, and R. W. Andrews (1985), Sensitivity analysis for steady state groundwater flow using adjoint operators, *Water Resour. Res.*, *21*(3), 359–371, doi:10.1029/WR021i003p00359.

Theis, C. V. (1935), The relation between the lowering of the piezometric surface and the rate and duration of discharge of a well using groundwater storage, *Eos Trans. AGU*, *2*, 519–524.

Thiem, G. (1906), *Hydrologische Methoden*, 56 pp., Gebhart, Leipzig, Germany.

Tiedeman, C. R., and P. A. Hsieh (2004), Evaluation of longitudinal dispersivity estimates from simulated forced- and natural-gradient tracer tests in heterogeneous aquifers, *Water Resour. Res.*, *40*, W01512, doi:10.1029/2003WR002401.

Tosaka, H., K. Masumoto, and K. Kojima (1993), Hydropulse tomography for identifying 3-D permeability distribution, paper presented at 4th Annual International Conference on High Level Radioactive Waste Management, Am. Soc. of Civ. Eng., Las Vegas, Nev., 26–30 April.

Tronicke, J., K. Holliger, W. Barrash, and M. D. Knoll (2004), Multivariate analysis of cross-hole georadar velocity and attenuation tomograms for aquifer zonation, *Water Resour. Res.*, *40*, W01519, doi:10.1029/2003WR002031.

Vasco, D. W., and A. Datta-Gupta (1999), Asymptotic solutions for solute transport: A formalism for tracer tomography, *Water Resour. Res.*, *35*(1), 1–16, doi:10.1029/98WR02742.

Vasco, D. W., H. Keers, and K. Karasaki (2000), Estimation of reservoir properties using transient pressure data: An asymptotic approach, *Water Resour. Res.*, *36*(12), 3447–3465, doi:10.1029/2000WR900179.

Yeh, T.-C. J., and C.-H. Lee (2007), Time to change the way we collect and analyze data for aquifer characterization, *Ground Water*, *45*(2), 116–118, doi:10.1111/j.1745-6584.2006.00292.x.

Yeh, T.-C. J., and S. Liu (2000), Hydraulic tomography: Development of a new aquifer test method, *Water Resour. Res.*, *36*(8), 2095–2105, doi:10.1029/2000WR900114.

Zanini, A., and P. K. Kitanidis (2008), Geostatistical inversing for large-contrast transmissivity fields, *Stochastic Environ. Res. Risk Assess.*, in press.

Zhu, J., and T.-C. J. Yeh (2006), Analysis of hydraulic tomography using temporal moments of drawdown recovery data, *Water Resour. Res.*, *42*, W02403, doi:10.1029/2005WR004309.

T. Clemo, Center for Geophysical Investigation of the Shallow Subsurface, Boise State University, 1910 University Drive, Boise, ID 83725-1536, USA. (tomc@cgiss.boisestate.edu)

M. N. Fienen, Wisconsin Water Science Center, U.S. Geological Survey, 8505 Research Way, Middleton, WI 53562, USA. (mnfienen@usgs.gov)

P. K. Kitanidis, Civil and Environmental Engineering, Stanford University, The Jerry Yang and Akiko Yamazaki Environment and Energy Building, Mail code 4020, 473 Via Ortega, Stanford, CA 94305, USA. (peterk@stanford.edu)